Molecular microelectrostatic view on electronic states near pentacene grain boundaries

Stijn Verlaak and Paul Heremans
IMEC, Kapeldreef 75, B-3001 Leuven, Belgium
(Received 19 November 2006; published 27 March 2007)

Grain boundaries are the most inevitable and pronounced structural defects in pentacene films. To study the effect of those structural defects on the electronic state distribution, the energy levels of a hole on molecules at and near the defect have been calculated using a submolecular self-consistent-polarization-field approach in combination with atomic charge-quadrupole interaction energy calculations. This method has been benchmarked prior to application on four idealized grain boundaries: a grain boundary void, a void with molecules squeezed in between two grains, a boundary between two grains with different crystallographic orientations, and a grain boundary void in which a permanent dipole (e.g., a water molecule) has nested. While idealized, those views highlight different aspects of real grain boundaries. Implications on macroscopic charge transport models are discussed, as well as some relation between growth conditions and the formation of the grain boundary.

DOI: 10.1103/PhysRevB.75.115127 PACS number(s): 77.22.−d, 71.23.An, 71.20.Rv

I. INTRODUCTION

Organic molecular single crystals have been studied for decades for their intriguing charge transport properties.[1–3] With the demonstration of organic electronic devices like transistors,[4] but also light-emitting diodes and solar cells,[5,6] charge transport in molecular thin films has gained increasing interest. Unlike nearly perfect crystals, charge transport in amorphous and polycrystalline thin films is dominated by various kinds of defects. In the present state of technology, many defects are extrinsic to the organic semiconductors used and are related to moisture,[7] impurities, e.g., as a result of chemical reactions,[8] hydroxyl groups at the SiO_2 surface acting as electron traps,[9] energetic disorder induced by random dipoles in the gate dielectric with which the semiconductor forms an interface,[10] etc. Other electronic defects find their origin in structural defects affecting the crystalline quality of the semiconductor film or crystal,[11–16] and are more intrinsic to film or crystal formation processes. Those latter defects as well can have considerable impact on both molecular energy levels and intermolecular charge-transfer probability.

Descriptions of charge transport in thin films and their devices differ by their assumptions with respect to the spatial and energetic distribution of electronic defects. When defects are homogeneously distributed in space with densities comparable to the total density of states (e.g., in an amorphous film), charge transport can be described in terms of variable-range hopping:[17] charges hop from site (defect) to site (defect), the probability of each hop depending on the site-energies and the hopping distance. When defects are homogeneously distributed in space with densities significantly smaller than the total density of states, charge transport can be described by a multiple trapping and release model: charges move at their intrinsic "single-crystal" mobility (it is irrelevant whether this mobility is determined by band or hopping transport), but get occasionally trapped in a defect from which they can be released again by thermal activation.[18] Lastly, when defects are spatially concentrated, charge transport can be described by a grain boundary model. Charges will concentrate at the defects, and depending on their sign they will form a potential barrier or a potential well for majority carriers traveling across the boundary.[19–21]

Those three models illustrate that an accurate description of charge transport hinges upon the detailed picture of the spatial and energetic distribution of electronic defects in thin films. Experimentally, all three models can fit pentacene transistor characteristics when the defect density of states is considered as a fit parameter.[21–27] The success of a fit therefore cannot be considered a distinguishing physical argument to select one or the other charge transport model. Some experimental data, such as the grain size and channel length dependence of transistor characteristics, can only be conveniently explained by grain boundary models.[21,26,28] Those effects are not always observed,[29,30] however, and it is not entirely clear under which intrinsic or extrinsic conditions they can be reproduced. In addition, such observations are often obscured by the fact that the first monolayer of pentacene, which is the layer transporting most charges in a field-effect transistor,[31–33] often has a morphology different from upper layers (which are the ones usually observed).[34]

Since it is difficult to shine light on the nature by which defects hinder charge transport in organic thin film transistors by experiment, a complementary approach tries to imagine the spatial and energetic distribution of electronic defects in such films *ab initio*. Idealistically assuming that extrinsic defects can be eliminated or at least significantly reduced technologically, electronic defects due to structural imperfections created during film growth come into focus. A previous study based on molecular mechanical calculations[35] shows that bulk defects are created during growth only in negligible quantities. Grain boundaries on the other hand are unavoidable and are suggested to be the dominant source of defects. In addition, compressive stresses at grain boundaries may give rise to dislocations and other imperfections inside the grains. The present work studies the electronic nature of grain boundaries in more detail. Since a grain boundary is a complex structure, various aspects of idealized situations will be studied to create a flavor of relevant mechanisms by which grain boundaries affect energy levels and charge trans-

port. The energy level of a charge on each of the molecules near a grain boundary will be calculated using well-established microelectrostatic methods. Similar methods have been used before for a variety of organic molecular semiconductors to study the electronic structure in single crystals and near voids,[36,37] dislocations,[38,39] chemical impurities,[40] surfaces, and interfaces.[41,42]

II. THEORY

Charge transport in an organic molecular crystal, being a sequence of transfers of an excess charge on one molecule to one of its neighboring molecules, is a relatively slow process at room temperature. As a matter of fact charges move so slow that they are able to polarize their environment before having the opportunity to transfer to another molecule: they induce dipoles in the surrounding molecules and promote nuclear relaxation mostly within the molecules on which they are localized. In addition to this electronic polarization and nuclear relaxation, charges can be screened or repelled by permanent electric quadrupoles on nearby molecules. Particularly polycyclic aromatic hydrocarbon molecules such as pentacene can electrically be viewed as quadrupoles, i.e., a positively charged planar backbone of atom cores with negatively charged π-electrons swarming out in front and in back of this plane. Consequently, charges never travel alone: they have to drag an electronically polarized environment, the interaction with permanent electric quadrupoles in the environment, and the intramolecular nuclear relaxation with them. The relevant quasiparticle to transport is therefore called a "nearly-small molecular polaron."[1–3] In the following, only positively charged polarons are considered. The conversion of the presented energy values to the energies of negative excess charges is straightforward and can be found in Ref. 1.

This interaction energy between the charge and the induced dipoles on neighboring molecules (polarization energy $E_{q\text{-}id}$), the interaction energy between the charge and the permanent quadrupoles of the neighboring molecules ($E_{q\text{-}Q0}$), and the nuclear relaxation energy (E_b), make up most of the difference between the energy of a positive nearly small molecular polaron in a crystal (i.e., the crystal ionization energy, IE_c) and the gas phase ionization energy (IE_g):[1]

$$IE_c = IE_g - E_{q\text{-}id} - E_{q\text{-}Q0} - E_b \quad (1)$$

E_b was estimated to be around −0.18 eV for pentacene.[43] The sum of the former two contributions, $E_{q\text{-}id}+E_{q\text{-}Q0}$, is often called the "apparent polarization energy." Note that here the convention was adopted that a free hole in vacuum has zero energy. The ionization energy is taken negative, as well as all energies that stabilize holes. In an ideal crystal, the crystal ionization energy IE_c of each equivalent molecule is identical. In the neighborhood of a defect, however, the ionization energy IE_i can vary from molecule to molecule since each molecule sees a different environment. The difference between the ionization energy of a molecule i, IE_i, and the ideal crystal ionization energy IE_c, is mostly determined by the difference in apparent polarization energy:

$$\Delta IE = IE_c - IE_i \approx E_{q\text{-}id,i} - E_{q\text{-}id,c} + E_{q\text{-}Q0,i} - E_{q\text{-}Q0,c} \quad (2)$$

since IE_g and E_b are dominated by intramolecular processes and hence will not differ for charges on different molecules with different environments. If ΔIE is positive, holes are more stabilized on a molecule in an ideal crystal than on a molecule in the vicinity of a defect. The latter molecules will therefore preferentially not be occupied by holes and act as scatter centers. If ΔIE is negative, the molecule in the vicinity of a defect will trap holes.

Given experimental values for IE_g, the problem of determining the energy (or electronic density of states) of a charge carrier on a molecule i near any arbitrary configuration of molecules in a solid is now reduced to determining the apparent polarization energy $E_{q\text{-}id,i}+E_{q\text{-}Q0,i}$. The microelectrostatic theory and the constants used here to calculate the apparent polarization energy are repeated and commented on in the appendixes of this text with consistent use of Système International units to avoid ambiguity and aid reproduction. In general, an excess charge on one molecule creates an electric field that induces dipoles on neighboring molecules. The induced dipoles are not only influenced by the electric field of the excess charge, but also by the electric fields of other induced dipoles. Therefore the electric field and the induced dipoles need to be solved self-consistently to calculate $E_{q\text{-}id}$. Several methods distinguish themselves from each other mostly by their representation of the polarizable molecules. A molecule can be represented by one point polarizable entity,[1] by a collection of artificially chosen point polarizable "submolecules,"[44,45] by one point polarizable entity at each (carbon) atom,[36] or ultimately by a "bag" of electrons that not only accounts for atomic polarizability but also for molecular charge redistribution over the extended π-system.[46] This last method automatically accounts for atomic multipolar contributions to electronic polarization, i.e., mostly charge-quadrupole interactions. Former methods all need to calculate the charge-quadrupole interaction energy $E_{q\text{-}Q0}$ separately by representing a molecule as a collection of permanent quadrupoles in much the same way as they represented molecules as a collection of point polarizable entities.

In this work, a submolecular approach was chosen. A pentacene molecule is represented by five point-polarizable entities distributed evenly along the molecular long axis to calculate $E_{q\text{-}id}$.[37] To calculate $E_{q\text{-}Q0}$, the molecular permanent quadrupole moment was distributed equally over all the 22 sp_2-hybridized carbon atoms of pentacene (i.e., each carbon atom represents a submolecule of the whole pentacene molecule), for all molecules in the environment of the charged molecule. An environment of approximately 320 molecules around the charged molecule (i.e., all molecules within a radius of 50 Å for a monolayer aggregate) was used to calculate ΔIE in the results section of this work. The Siegrist polymorph is used to construct the environment, see Table I. Differences between IE_c and IE_i due to contributions from molecules outside this radius are negligible. To calculate IE_c for benchmarking purposes, an enlarged environment of 530 molecules was involved in the calculation (i.e., all molecules within a radius of 65 Å for a monolayer aggregate, or all molecules within a radius of 35 Å for a three-dimensional

TABLE I. Presently calculated electronic polarization energies and charge-quadrupole energies for a hole in an infinitely large pentacene or anthracene crystal or monolayer and their comparison with literature values. In between brackets is the number of submolecules s used for the calculation. If s equals the number of atoms in one molecule (24 for anthracene and 36 for pentacene), atomic contributions to polarizability and higher order multipoles have been used. If s equals the number of π-atoms in one molecule (14 for anthracene and 22 for pentacene), the molecular polarizability and quadrupole moment has been equally distributed over all sp_2-hybridized carbon atoms. If s is a smaller number, the molecular polarizability and quadrupole moment has been equally distributed over s points along the molecular long axis. Scaling relations for extrapolation are indicated in the Appendixes.

Case	$E_{q\text{-}id}$ (s) (eV)	$E_{q\text{-}Q0}$ (s) (eV)	Method
Bulk pentacene, Campbell *et al.* crystal structure (a=6.06 Å, b=7.90 Å, c=14.88 Å, α=96.74°, β=100.54°, γ=94.2°) (Ref. 68)			
Hole at position (0,0,0)	−1.075 (5)	−0.215 (5)	Fourier transform (Ref. 37)
Hole at position (1/2,1/2,0)	−1.069 (5)	−0.240 (5)	Fourier transform (Ref. 37)
Hole at position (0,0,0)	−1.007 (36)		Extrapolated SCPF with charge redistribution (Ref. 42)
Hole at position (1/2,1/2,0)	−1.0035 (36)		Extrapolated SCPF with charge redistribution (Ref. 42)
Hole at position (0,0,0)	−1.157 (5)	−0.205 (5)	$E_{q\text{-}id}$ by extrapolated SCPF
		−0.258 (22)	$E_{q\text{-}Q0}$ at R=35 Å (present work)
Hole at position (1/2,1/2,0)	−1.158 (5)	−0.273 (5)	$E_{q\text{-}id}$ by extrapolated SCPF.
		−0.321 (22)	$E_{q\text{-}Q0}$ at R=35 Å (present work)
Bulk pentacene, Siegrist *et al.* crystal structure (a=6.27 Å, b=7.79 Å, c=14.51 Å, α=76.65°, β=87.5°, γ=84.61°) (Ref. 69)			
Hole at position (0,0,0)	−1.181 (5)	−0.251 (5);	$E_{q\text{-}id}$ by extrapolated SCPF
		−0.292 (22)	$E_{q\text{-}Q0}$ at R=35 Å (present work)
Hole at position (1/2,1/2,0)	−1.186 (5)	−0.223 (5);	$E_{q\text{-}id}$ by extrapolated SCPF
		−0.303 (22)	$E_{q\text{-}Q0}$ at R=35 Å (present work)
(001) monolayer pentacene, Siegrist *et al.* crystal structure (Ref. 69)			
Hole at position (0,0,0)	−0.955 (5)	−0.524 (5);	SCPF ($R<65$ Å) and continuum polarization;
		−0.574 (22)	$E_{q\text{-}Q0}$ by extrapolation (present work)
Hole at position (1/2,1/2,0)	−0.961 (5)	−0.482 (5);	SCPF ($R<65$ Å) and continuum polarization;
		−0.530 (22)	$E_{q\text{-}Q0}$ by extrapolation (present work)
Bulk anthracene, Mason crystal structure (a=8.56 Å, b=6.04 Å, c=11.18 Å, α=90°, β=124.42°, γ=90°) (Ref. 70)			
Hole at position (0,0,0) or (1/2,1/2,0)	−1.53 (1)		SCPF and continuum polarization (Ref. 11)
Hole at position (0,0,0) or (1/2,1/2,0)	−1.193 (3);	−0.182 (3);	Fourier transform (Refs. 36 and 37)
	−1.162 (14)	−0.249 (14)	
Hole at position (0,0,0) or (1/2,1/2,0)	−1.1 (24)	−0.27 (24)	Extrapolated SCPF with charge redistribution (Refs. 71 and 72)
Bulk anthracene, Brock *et al.* crystal structure (a=8.41, b=5.99, c=11.10, α=90°, β=125.29°, γ=90°) (Ref. 73)			
Hole at position (0,0,0) or (1/2,1/2,0)	−1.320 (3)	−0.199 (3);	$E_{q\text{-}id}$ by extrapolated SCPF
		−0.264 (14)	$E_{q\text{-}Q0}$ at R=35 Å (present work)
Experimentally derived values (Ref. 43)			
Hole in pentacene	−1.22	−0.23	Experimental data interpreted by theoretical correlations (Ref. 43)
Hole in anthracene	−1.22	−0.28	Experimental data interpreted by theoretical correlations (Ref. 43)

crystalline aggregate). The contribution from molecules outside this radius can be extrapolated using the scaling laws described in the appendixes. Table I shows some benchmark results with this method, in comparison with other values in literature.

First, calculated values need to be compared with experimental data. Experimental values for IE_g and IE_c, as well as estimates for E_b based on experimental data, are listed in Ref. 43 for anthracene and pentacene. Inserting those values in Eq. (1), yields $E_{q\text{-}id}+E_{q\text{-}Q0}=-1.45\pm0.3$ eV for pentacene and -1.5 ± 0.3 eV for anthracene. For comparison, the calculated benchmark results with the present method in Table I yield -1.45 eV (averaged over both inequivalent molecules in the pentacene Campbell unit cell) and -1.58 eV, respectively. Individual values for $E_{q\text{-}id}$ and $E_{q\text{-}Q0}$ for pentacene and anthracene derived from the experimental data and correlations in Ref. 43 are listed as well in Table I.

Second, calculated values are compared to other calculations in literature. Table I presents the energies for charge carriers in infinitely large crystals. For the Fourier transform method, the infinite dimensions of the aggregate are implicit in the calculations. For other methods, results for finite aggregates have been extrapolated to infinite crystals according to the scaling relation in the appendixes of this text. Alternatively, a correction was calculated to the energy value of a charge carrier in a finite sized aggregate, assuming continuum polarization outside the aggregate as described in Appendix A. While using the same submolecular representation, molecular polarizability, and quadrupole moment tensors as in Ref. 37, our values differ by as much as 0.09 eV for $E_{q\text{-}id}$ and 0.03 eV for $E_{q\text{-}Q0}$ for bulk pentacene in the Campbell polymorph. This difference can be attributed partially to the extrapolated nature of our results, but mostly to slight differences in the molecular coordinate system, which was determined here by the molecular principal axes of inertia. The difference in $E_{q\text{-}id}$ is larger when compared to more elaborate calculations, and can amount up to 0.16 eV for pentacene. The difference in $E_{q\text{-}Q0}$ is rather small on the other hand when compared to atomic multipolar contributions for anthracene that mostly consist of charge-quadrupole interactions. This is not entirely surprising, since the accuracy of calculating charge-quadrupole interactions is highly improved by distributing the molecular quadrupole moment equally over all sp_2-hybridized carbon atoms (they are mostly π-electrons coming from sp_2-hybridized carbon atoms that contribute to the quadrupole moment), as was recognized in Ref. 36. Overall, the error on the calculations in the remainder of this work is significantly reduced, since only differences in apparent polarization energies will be considered.

Lastly, significant differences are observed between the charge-quadrupole interaction energy of a charge in one monolayer when compared to a charge in a bulk crystal. π-electrons of intralayer molecules are the predominant species to screen a positive excess charge inside the same monolayer: they can easily polarize and screen the excess charge (i.e., the effect of induced dipoles), and they shield the positive atomic cores of the molecule backbone from the excess positive charge (i.e., the effect of the molecular quadrupole). π-electrons of molecules in layers neighboring the excess charge, on the other hand, are much less susceptible to polarization (due to the fact that they are more distant from the excess charge). More important, however, is that the molecular quadrupoles in neighboring monolayers destabilize the excess positive charge because the electrons are much less effective in shielding the positive atomic cores of the molecular backbone from the excess positive charge.

III. RESULTS

The previous section justified the method to calculate the electronic states of charged molecules within any arbitrary environment. In this section, the effect of grain boundaries in pentacene thin films on the electronic state distribution will be studied. This distribution of electronic states provides the energetic landscape within which a charge will need to travel if it is to cross the grain boundary, e.g., for charges transported in a polycrystalline pentacene thin film transistor. Since grain boundaries come in many shapes and flavors, a number of idealized views on grain boundaries is selected here, each view highlighting a different characteristic of an arbitrary "real" grain boundary. By combining the quantitative and qualitative insights in those idealized views, the reader should be able to form an idea of what the electronic landscape near an arbitrary grain boundary can look like. The different idealized grain boundaries considered are

(a) a void between two aligned grains;
(b) a void filled by molecules in a nonideal crystal configuration;
(c) a boundary formed by two grains whose crystallographic orientations are misaligned; and
(d) a void filled with a permanently polarized molecule such as water that has penetrated the boundary.

In all cases, a boundary was constructed starting from a (110) pentacene monolayer edge. The (110) surface is the most stable in the Siegrist polymorph used here, and generally forms a dominant feature in grain shapes.[47,48]

All following results are produced as follows.

(1) A large monolayer aggregate is built for each idealized grain boundary.
(2) A charge is placed on a molecule i within the aggregate.
(3) All molecules within a radius of 50 Å surrounding the charged molecule are selected from the aggregate to calculate ΔIE according to the procedure outlined above.
(4) The procedure is repeated by placing the charge on each molecule of interest. Note that the monolayer aggregate constructed in (1) should be large enough to contain not only the molecules on which the charge will be placed to calculate ΔIE, but also at least all molecules within 50 Å surrounding those molecules.

A. Grain boundary voids

Grains of pentacene thin films grown on an inert amorphous substrate such as PEDOT, SiO_2, or any other dielectric

substrate, nucleate in a random way. Not only are the crystallographic orientations of the different nuclei randomly distributed, but also their positions lack any correlation due to the absence of an underlying crystalline lattice as in epitaxial growth. The latter aspect will be studied in this paragraph and the next. This paragraph studies two neighboring grains that have the same crystallographic orientation, but whose positions can shift relatively to each other by a fraction of a unit cell length, as in Figs. 1(a) and 1(b). The boundary interface between those grains will often form a void for one or a combination of the following reasons.

(1) There is not enough space at the interface to squeeze in another molecule. Even if there can still be molecules squeezed in between the grains, they will not be at an ideal pentacene lattice site, and the total density of molecules squeezed in between the grains will always be lower than the density of molecules in an ideal pentacene crystal. Those voids are difficult to avoid on inert and/or amorphous substrates. They are somewhat easier to avoid in (quasi-) epitaxial growth.

(2) The pentacene grains have nucleated in a three-dimensional islandlike fashion,[47] and when growing together, the probability for a molecule to fill the gap between the two bulky islands becomes smaller. Those voids can often be filled by increasing the flux and/or decreasing the substrate temperature.[47,49]

Such voids were experimentally found to hinder charge transport.[49] In this work, lattice relaxation around grain boundaries is excluded from the analysis. In the case of grain boundary voids, little relaxation is expected in the absence of long-range attraction forces.[50] Indicatively, hardly any relaxation was found near vacancies in ideal organic crystals.[51,52]

Figure 1(b) shows the variation of ΔIE [the difference in energy of a positive charge in an ideal crystalline pentacene monolayer, and a charge on each molecule of Fig. 1(b)] near a grain boundary void. Given the lower density of molecules near the void, there are less π-electrons in the neighborhood to screen a positive charge, and such a charge is destabilized near the boundary. The molecules at each side of the interface will scatter holes, and form an implicit energy barrier. If a charge is to cross the boundary, it will have to cross this energy barrier. For large voids, such as in Fig. 1(b), a charge is hindered even more in its travel by the strongly reduced electronic coupling between molecules on each side of the interface. Striking in Fig. 1(b) is the large difference in ΔIE: on some molecules at the boundary, a hole would be destabilized by 0.33 eV, while on other molecules, it will be destabilized by only 0.09 eV. This is related to the anisotropy of the polarizability tensor and the quadrupole moment (see Appendixes A and B), as illustrated in Fig. 2. The charge-quadrupole interaction in particular is responsible for the large difference between molecules with ΔIE=0.09 eV and those with ΔIE=0.33 eV, as can be clearly seen in Fig. 2(b): if a molecule neighboring a hole (a positively charged molecule) has a quadrupole moment such that it shows its negatively charged face to the hole, it will help stabilize the hole. Therefore in Fig. 1(b), a hole on molecule 2 will be screened by the quadrupole moment of molecule 1. On the other hand,

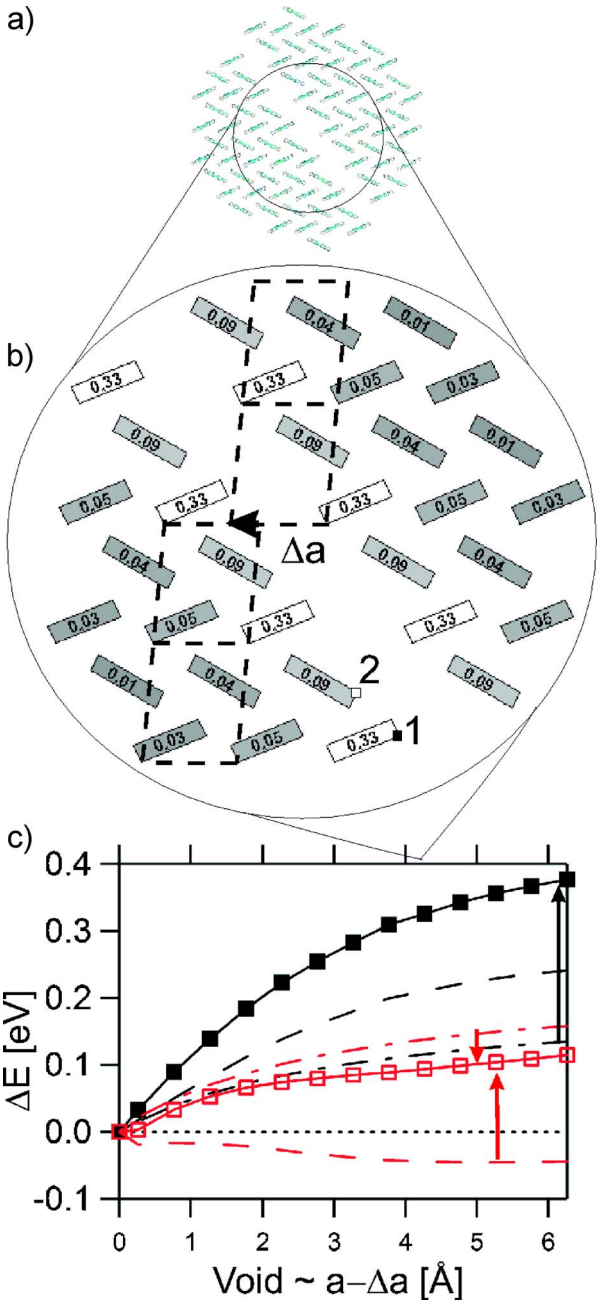

FIG. 1. (Color online) (a) The grain boundary void is viewed along the molecular long axes. (b) The molecules near the grain boundary with a void of a−2 Å=4.265 Å form alternating scatter centers of 0.07 and 0.41 eV. The molecules are sketched along the projection of their medium molecular axis on the paper. (c) The formation of scattering centers is reduced when the void is closed by moving the two grains by a distance Δa towards each other. Shown is ΔIE (filled squares) for the strongest scattering center at the boundary, ΔIE (empty squares) for the weakest scattering center at the boundary, and their components $\Delta E_{q\text{-}id}$ (dash-dotted line) and $\Delta E_{q\text{-}Q0}$ (dashed line).

if a molecule faces the hole with its positive backbone, it will destabilize the hole. In Fig. 1(b), a hole on molecule 1 will be repelled by the quadrupole moment of molecule 2. To further illustrate this case, and to give an indication of the variation in energetic landscape near grain boundaries, ΔIE

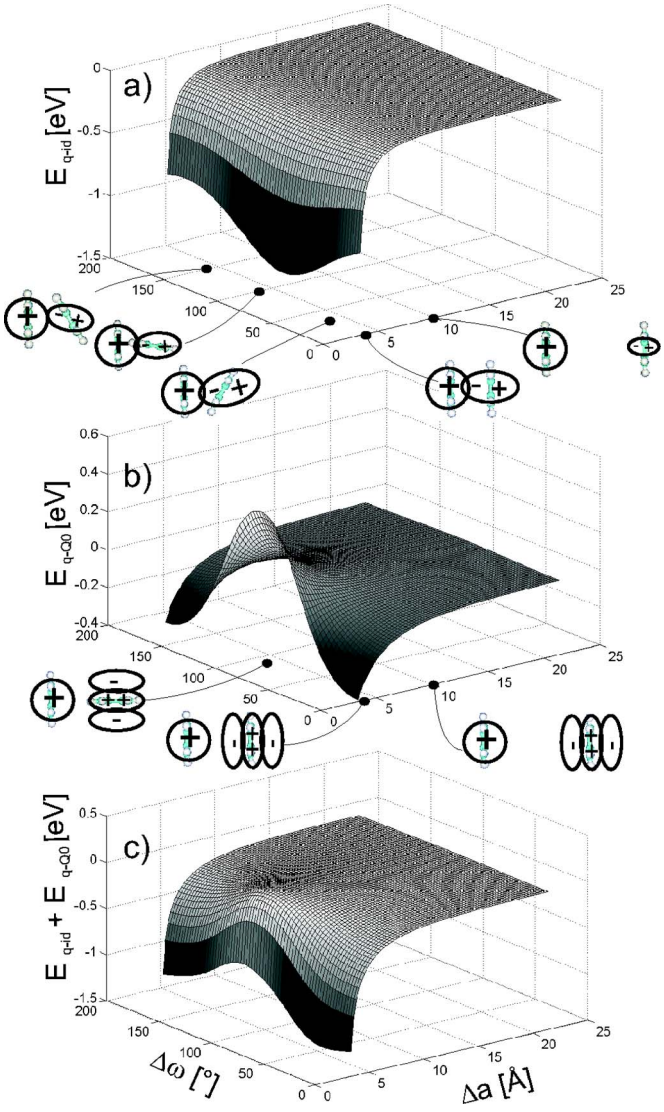

FIG. 2. (Color online) Distance and orientation dependence of (a) the electronic polarization energy $E_{q\text{-}id}$, (b) the charge-quadrupole interaction energy $E_{q\text{-}Q0}$, and (c) the total apparent polarization energy $E_{q\text{-}id}+E_{q\text{-}Q0}$ for a two-molecule system. The positively charged molecule is fixed in space and indicated by a "+." The other molecule is at a distance Δa from the first and rotates around its long axis by $\Delta\omega$.

is shown for an (010) pentacene grain boundary in Fig. 3. Near that interface, all holes are equally repelled. Moreover, the effect of the void is felt over a longer distance from the boundary when compared to Fig. 1(b).

Figure 1(c) summarizes the evolution of the weakest and strongest scatter centers at the (110) boundary interface for decreasing voids. It is seen that the electronic polarization is always smaller than in an ideal crystalline monolayer ($\Delta E_{q\text{-}id}$ is positive), due to the smaller number of π-electrons to polarize in the neighborhood of the void. The charge-quadrupole interaction on the other hand, can be both positive or negative, as also explained above, and can exceed the magnitude of the electronic polarization.[37]

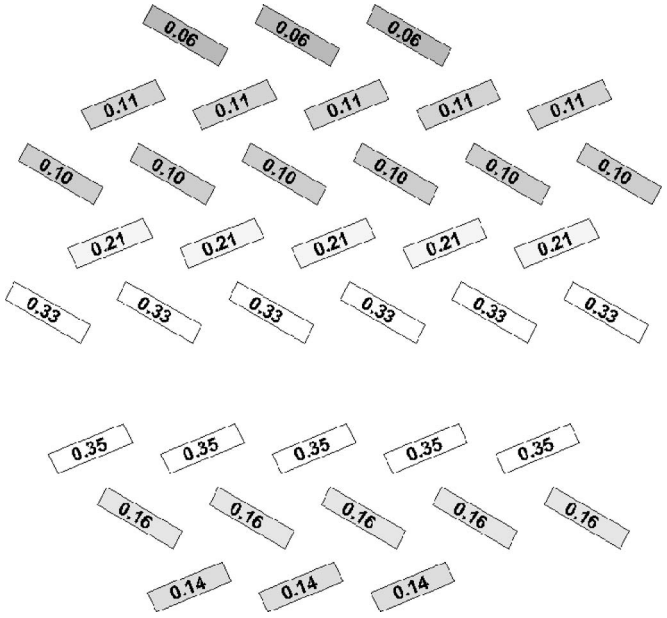

FIG. 3. Apparent polarization energy differences Δ*IE* (eV) near a pentacene (010) grain boundary void of width b−4 Å=3.79 Å (measured along the b axis).

B. Filled grain boundary voids

When the void separating two grains is still large, it will be fairly easy to squeeze some molecules in between the grains. "Fairly easy" can be quantified by the sum of the intermolecular interactions between this squeezed-in molecule and its nearest neighbors, i.e., the structural interaction energy. The lower (i.e., the more negative) the structural interaction energy for a molecule in a particular position, the more a molecule likes to sit in that position. Figure 4 illustrates the variation in the structural interaction energy of one molecule squeezed in between two grains in its most stable position, with varying voids between the grains. The calculational procedure for this graph is described elsewhere.[35] The dashed line demarcates the structural interaction energy of molecules that would still have a 50% probability to occupy a state with that energy in between two grains at zero supersaturation. States with energies higher than the demarcation line can only be formed at higher supersaturations, that is higher deposition fluxes or lower substrate temperatures.[35] Typical supersaturations in pentacene film growth experiments are a few tenths of an eV.[47] In practice, that would mean that the void with $\mathbf{a}-\Delta a=4.265$ Å can still be filled with molecules at moderate supersaturations, while smaller voids remain empty like in the previous paragraph [for the definition of Δa, please refer to Fig. 1(b)]. This demonstrates that growth conditions can have a pronounced effect on the formation of grain boundaries and their electronic landscape.

Figure 5 shows the hole energies relative to the ideal crystal transport energy (i.e., Δ*IE*) for molecules near filled boundaries. In all cases, moderate to deep traps (negative Δ*IE*) are formed along some point of the minimum-energy path that will be followed by a hole traveling across the boundary. Also here, the charge-quadrupole energy is largely

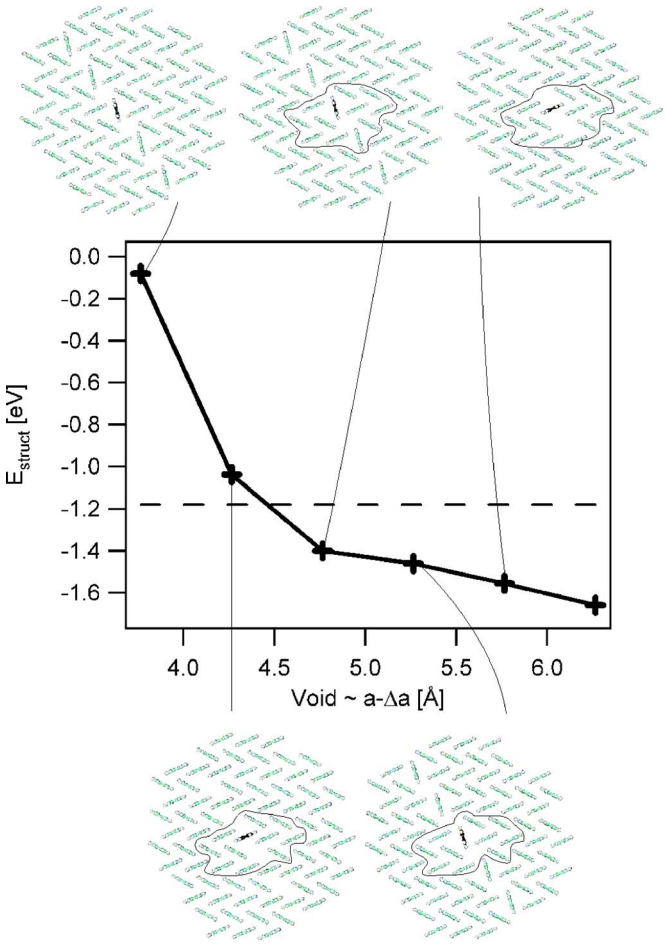

FIG. 4. (Color online) Structural interaction energy E_{struct} of one molecule squeezed in a grain boundary void. The width of the void is $a-\Delta a$ as in Fig. 1, and ranges from $a-2.5$ Å, $a-2.0$ Å, $a-1.5$ Å, $a-1.0$ Å, $a-0.5$ Å to $a-0.0$ Å, with $a=6.265$ Å. The dashed line indicates the structural interaction energy level at which a molecule would still be stable at zero supersaturation. Molecules with higher structural interaction energies will only be squeezed in between the grains at higher supersaturations (higher deposition flux or lower substrate temperature).

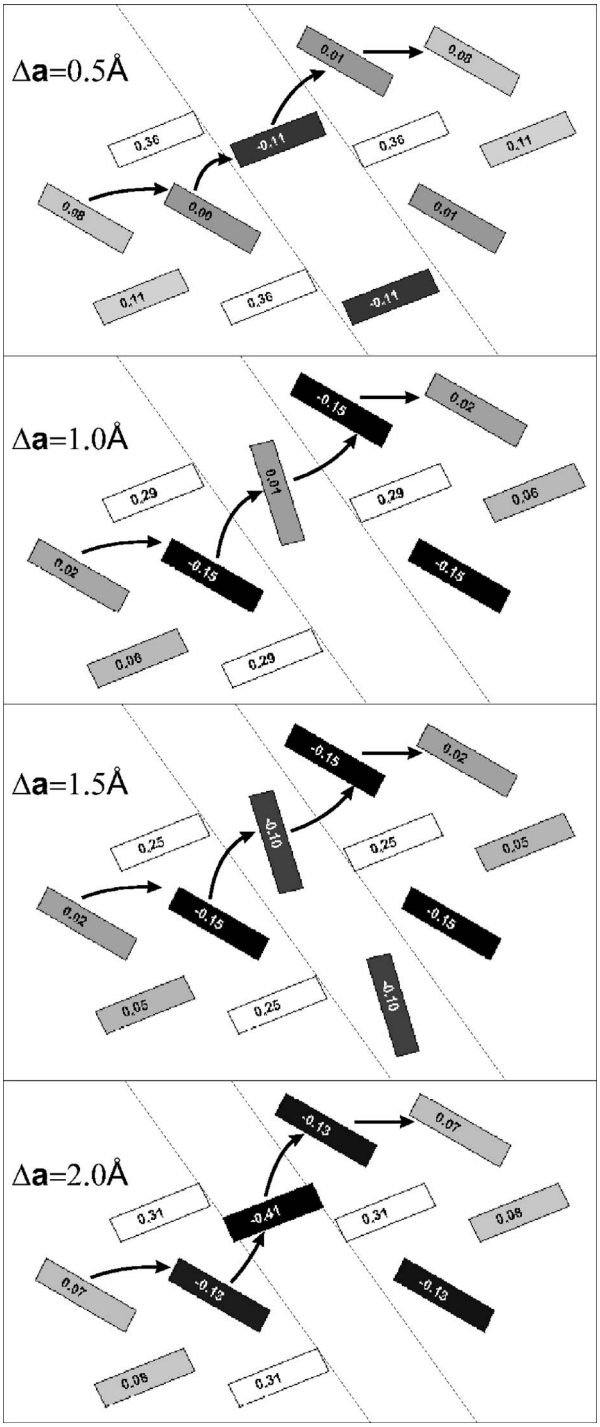

FIG. 5. Hole energies ΔIE (relative to the ideal crystal transport energy) near filled grain boundaries (for the molecules demarcated in Fig. 4). The minimum-energy path for charge transport is indicated by arrows. The dotted lines are a guide to the eye, demarcating the void between the two grains.

responsible for the creation of traps and scatter centers. In conjunction with the above discussion about the likeliness of filling voids at grain boundaries with molecules, it can be concluded that a higher supersaturation on average will lead to an increased filling of the grain boundaries and the concomitant creation of hole trap states. At lower supersaturation, more grain boundaries will remain empty, forming hole scatter centers as in the previous paragraph.

C. Boundaries along misaligned grains

Assume that the crystallographic orientation of a grain is already determined by the nucleation event, that this orientation is moreover randomly distributed over all nuclei on an amorphous substrate, and that this orientation is maintained upon the growth of the nucleus. A grain will continue growing until it meets a neighboring grain, with which it will form a boundary. This boundary will separate two grains with different crystallographic orientations.

Such boundaries have been constructed in Fig. 6. The proximity of the grain at the right with respect to the grain at the left has been optimized using the MM3 molecular mechanics forcefield using similar procedures as described in

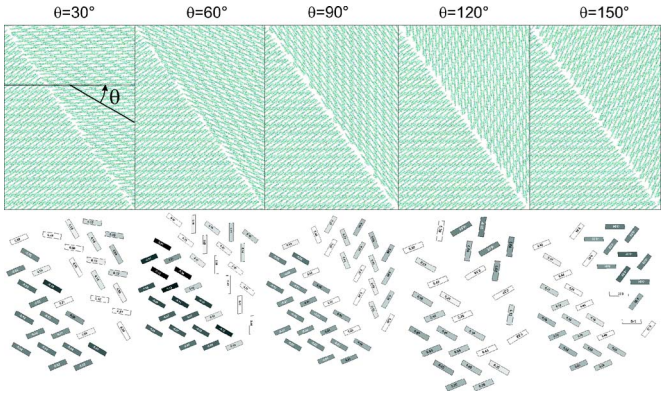

FIG. 6. (Color online) Boundaries between misaligned grains. Below are the hole energies relative to the ideal crystal transport energy (ΔIE). States with energies $\leqslant -0.25$ eV (traps) are indicated in black, those with energies $\geqslant 0.25$ eV (scatter centers) are white.

Ref. 35. This optimization prevents indentation of the two grains, or alternatively that they would be spaced too far away from each other. Note that during this optimization the grain at the right was considered as a rigid block, i.e., no relaxation has been taken into account. In reality, the orientation mismatch at the interface between crystalline grains of small organic molecules can be optimized by bending the crystal orientations somewhat towards the interface to permit an optimum number of van der Waals contacts between molecules (but there will still remain an orientation mismatch).[53] This will not affect the following qualitative discussion.

From a bird's eye view, the grayscale values of the hole energies in Fig. 6 gradually shift from trap energies in the grain at the left and scatter centers in the grain at the right at $\theta=30°$, towards trap energies in the grain at the right and scatter centers in the grain at the left at $\theta=150°$. Also here, the charge-quadrupole interactions dominate the trap or scatter energies. The results can qualitatively be explained by realizing the following.

(1) The charge-quadrupole interaction is not reciprocal. If a charge on one molecule is stabilized by the permanent quadrupole on another molecule, then a charge on the latter molecule would be destabilized by the permanent quadrupole on the first molecule, as already discussed in Sec. III A and Fig. 2. This explains why one side of the grain boundary seems to consist of mostly traps, while the other side consists of mostly holes.

(2) The average orientations of the molecules and their quadrupole moments in the misaligned grain differ substantially when compared to the boundaries studied in Secs. III A and III B. Note that even the molecules squeezed in between two grains still had their molecular long axis parallel to the molecular long axes of molecules in the two grains, while in the misaligned grain even the molecular long axes have changed orientation. This explains the gradual shift of trapping versus scattering pattern when the crystalline orientation of the grain at the right is rotated by $\theta=30°$–$150°$.

In addition to those effects, it should be noted that contrary to previous grain boundary structure, the boundaries in this section are no longer periodic in a short range. As a result, there is a substantial variation in hole energies along the interface on a length scale somewhat longer than shown at the bottom of Fig. 6. For example, for $\theta=60°$, the energy of holes on molecules at the left side of the interface varies from −0.36 to 0.25 eV (not shown here) relative to the ideal crystal transport energy.

Misaligned grain boundaries can be avoided using specific growth methodologies. Controlled step-edges of about one molecule high can be used not only to induce nucleation, but also to guide the crystallographic orientation of the nuclei along the edge.[54] In much the same way as pentacene grows in monolayers on inert substrates because the (001) crystal face has the lowest surface energy,[55] grains are expected to nucleate along a step edge with their lowest crystal face [next to the (001) face] parallel to the edge.[47] Consequently, along the step edge, all grains will have the same crystallographic orientation.

D. Permanent dipoles at grain boundaries

Some polycrystalline organic small-molecular transistors have been used as humidity or odor sensors.[56–58] In both cases, the sensing effect was attributed to water or other molecules diffusing into the devices along the grain boundaries. Because the grain boundaries run almost all the way down to the first few monolayers on the substrate, such molecules can electrostatically interact there with the charges in the transistor channel, creating energetic disorder through charge-dipole interactions.[56] In a similar way but beyond the scope of this work, it was suggested that polar dielectric substrates would increase the energetic disorder of charges in an organic film by charge-dipole interactions.[10]

To get some feeling for the effect of permanent dipoles, the apparent polarization energy was calculated in Fig. 7(a) for a grain boundary with a void of $\mathbf{a}-2.5$ Å [cf. Fig. 1(b), with **a** the unit cell axis of the pentacene crystal which is here 6.265 Å long along the x axis] in which one water molecule was placed with its permanent dipole aligned along the **a** axis. The permanent dipole not only interacts directly with a charge in its vicinity, but also influences the direction and magnitude of induced dipoles on neighboring pentacene molecules. Increasing the dipole moment does lead to a clear broadening of the distribution of states in Fig. 7(b). The largest contribution is by far the charge-permanent dipole interaction, sometimes reinforced by −0.05–0.2 eV by the charge-permanent quadrupole interaction, while differences in charge-induced dipole interactions stay limited to 0.02–0.1 eV. Note however, that the distribution of states in Fig. 7(b) is correlated (i.e., there is a progressive evolution towards the largest scatter centers and the deepest traps when moving from the grain to the boundary) and should not be interpreted as a density-of-states distribution in the context of a model like a variable range hopping model. Rotating the water molecule in Fig. 7(c) does not significantly affect the distribution of states, apart from the two states closest to and along the direction of the permanent dipole. It should be noted that the effect of just one permanent dipole at the interface is still different from a distribution of dipoles at the boundary interface. However, if dipoles come closer to-

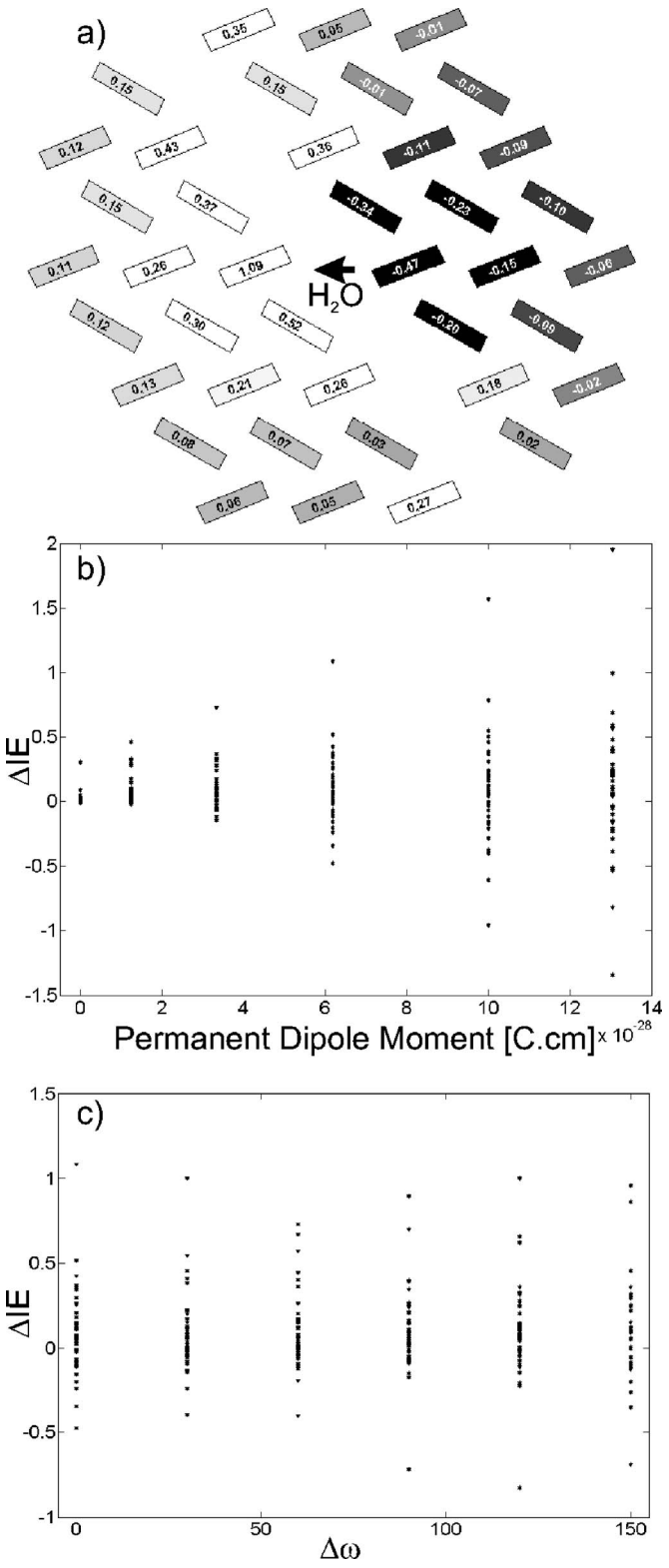

FIG. 7. Effect of permanent dipoles on the energetic landscape near a grain boundary: (a) spatial distribution for a water molecule with a permanent dipole aligned at $\Delta\omega=0°$ with the a axis; (b) change in distribution of states with increasing permanent dipole moment. For a given dipole moment on the abscissa, the energy for a charge placed on each of the molecules of the aggregate in (a) is plotted as a point along the ordinate; and (c) change in distribution of states by rotating the water molecule in the grain boundary.

gether, they will try to align in opposite directions and partially cancel their effect on the electronic density-of-states distribution. Expectations are therefore that on average the density-of-states distribution will not get broader when comparing a distribution of permanent dipoles to just one permanent dipole at the boundary.

IV. DISCUSSION

The results presented above describe the energetic landscapes of a positive charge near some idealized grain boundaries. In this section, the implications of that description for a macroscopic charge-transport model in polycrystalline organic thin films will be discussed.

First of all, from the results presented here, it is possible to distinguish between two types of grain boundaries: those that form *intrinsic* barriers and those containing trapping centers. An intrinsic barrier is formed by grain boundaries consisting of scatter centers, like near a void. Near a void, the scatter centers will gradually become larger towards the void separating two grains. This situation represents an intrinsic energy barrier for the hole: the barrier is solely due to the arrangements of molecules near the grain boundary. Indicative values for the intrinsic barrier height are 0.1–0.4 eV [for voids at grain boundaries near aligned (110) and (010) interfaces, respectively, as in Figs. 1 and 3]. Note that the width of this intrinsic barrier is only a few nanometers wide, see, for example, Fig. 1(b). If the hole is to cross the boundary, it has to hop uphill in energy, site-by-site.

If a hole approaches a grain boundary that also contains trapping centers, it will get trapped. Following holes are repelled by the first hole. They will hop around the first hole and eventually get trapped at different locations along the grain boundary until an equilibrium occupation has been reached. Trapping more states at the grain boundary is not electrostatically possible without detrapping other holes. The whole grain boundary is charged by a front of trapped holes that repel other holes, i.e., it will increase the energy for holes on neighboring molecules. In other words: a potential barrier is formed. Both height and width of this potential barrier not only depend on the density of trapped charges, but also on the position and density of the negative countercharges necessary to keep the film electrically neutral.[19,21,59] Note that in the molecular approach presented here, charges are often funneled to one specific trapping site at the boundary, e.g., in Fig. 5, and that in many cases a monoenergetic trap level determines the equilibrium density of trapped charges and hence the barrier height.

In both cases, mobile holes need to move to the top of the potential barrier. The probability for a hole in the bulk of a grain (at the transport level) to gain enough thermal energy to reach the top of the potential barrier (i.e., on a molecule at the interface between the two grains), is given by Boltzmann statistics. The likeliness for a hole that has reached the top of the potential barrier to cross the grain boundary is strongly influenced by the electronic coupling between molecules on either side of the boundary and is reflected in the boundary-crossing charge-carrier mobility μ_{bc}. The overall mobility for a mobile hole in the bulk of a grain to cross the boundary μ_{gb}

is then a very similar expression as for polysilicon grain boundary barrier models:

$$\mu_{gb} = \mu_{bc} \exp\left(-\frac{\phi_b}{kT}\right), \tag{3}$$

with ϕ_b the barrier height (either the intrinsic barrier height or the potential barrier height), k the Boltzmann constant, and T the film temperature. The difference with the polysilicon model lies in the different interpretation of the mobility prefactor, μ_{bc}, which in the latter case is determined by the thermal velocity of charge carriers jumping over the barrier without scattering. Note that when the barrier is due to the potential raised by shallowly trapped carriers, the fastest way for a carrier to cross the boundary might alternatively be to get trapped and detrapped, in which case the net detrapping time determines the average mobility μ_{gb}.

So far, when looking at one specific boundary, it is found that the essential properties of such a boundary can be given by the intrinsic barrier height (if present), the monoenergetic trap level at the boundary interface (if present), and the rate-limiting cross-boundary hop mobility μ_{bc}. For a *single* hole to cross a *neutral* grain boundary, the barrier height ϕ_b (i.e., the activation energy for the hole mobility across that boundary) can be determined directly from the calculated values presented here. Figure 5, for example, demonstrates the most likely paths for a single hole to cross the various boundaries. For the first case ($\Delta a = 0.5$ Å), the rate-limiting steps for the hole to cross the boundary are given by the subsequent jumps from the molecule at $\Delta IE = -0.11$ eV to the molecule at $\Delta IE = 0.08$ eV, resulting in $\phi_b = 0.08 - (-0.11) = 0.19$ eV. Transistors, however, operate at fairly high charge densities. When the grain boundary forms an *intrinsic* barrier, no charges will be trapped at the boundary itself no matter how high the average charge densities inside the grains, and the barrier ϕ_b is still simply given by the values calculated here (e.g., Fig. 3 illustrates an intrinsic barrier of 0.35 eV to cross that particular grain boundary). In the most general case, however, grain boundaries also contain trapping sites. The filling of those trap sites will depend on the average charge density (i.e., on the gate voltage of the transistor). The potential barrier height ϕ_b will only be indirectly related to the energy levels near the boundary, and instead will be electrostatic in nature depending on the density of holes trapped at the boundary, as well as on the density and location of countercharges that screen the trapped holes.[21] In case of a polycrystalline thin-film transistor, for example, trapped holes at the grain boundary are screened by mobile negative charges on the gate. This negative charge at the gate reduces the effective potential barrier for mobile holes that cross the boundary. The latter problem can most efficiently be solved macroscopically, using a device simulator that solves for Poisson's and drift-diffusion equations. The present calculations can provide the necessary input for such a simulator, namely the distribution of trap states at the grain boundary interfaces. The present calculations are currently too limited in computing power to provide a direct microscopic answer for the barrier height ϕ_b in this multihole problem having a length scale of a few tens of a nanometers.

The main problem in describing charge transport in a polycrystalline *film* (when compared to describing the transport through just one grain boundary) lies in the averaging over the wide variety of grain boundaries that can be formed (often even with local variations along the boundary, as for the misaligned boundaries in Fig. 6). In reality, charge transport in polycrystalline organic films is a two-dimensional percolation problem, where currents will preferentially flow through the more permissive grain boundaries. An overview of percolation models and effective medium approaches is presented in Ref. 19, but concludes by stating that the true role of percolation in the transport properties of inhomogeneous semiconductors is difficult to ascertain. Note that the variety of grain boundaries formed depends on growth conditions. As mentioned earlier, higher supersaturations (larger deposition flux and lower substrate temperatures) promote the filling of grain boundaries, such that on average a smaller number of grain boundaries is expected to display voids, and a larger number of boundaries will contain trap centers.

V. CONCLUSIONS

To conclude, the energetic landscape for a hole traveling in a variety of idealized pentacene grain boundary cases has been studied on a microscopic scale, using self-consistent polarization fields as well as charge-quadrupole interactions. The electronic states near grain boundaries are found to form intrinsic energy barriers in many cases, but can also include trapping centers. Trapped holes at the boundary interface can in turn raise a potential barrier hindering charge transport for mobile holes across the grain boundary. In all cases, the charge-quadrupole interaction is dominant in determining the energy level. In some cases, the electronic states distribution near the boundary is clearly dependent on the growth conditions of the pentacene film.

The localized molecular picture helps to unveil the details of electronic state formation and its dependency on molecular, structural, and defect properties, as well as film growth conditions. The challenge is now to translate this microscopic view into a macroscopic continuum description of charge transport in polycrystalline organic films.

ACKNOWLEDGMENTS

S.V. would like to thank David Beljonne, Robert W. Munn, and Vladimir Arkhipov for useful and stimulating discussions and Jan Genoe, Cédric Rolin, David Cheyns, and Soeren Steudel for their reflections upon this paper. This work was supported by the EU Integrated Project NAIMO (No. NMP4-CT-2004-500355).

APPENDIX A: SELF-CONSISTENT POLARIZATION FIELDS

When an excess charge q is placed in a neutral matrix, it will generate a monopole electric field at point $\mathbf{r}$ at a distance $r = \sqrt{\mathbf{r} \cdot \mathbf{r}}$ from the charge, with vector $\mathbf{F_m}(\mathbf{r})$:[60]

$$\mathbf{F_m}(\mathbf{r}) = \frac{q}{4\pi\epsilon_0}\frac{\mathbf{r}}{r^3}, \tag{A1}$$

with ϵ_0 the permittivity of vacuum. If a polarizable point with polarizability volume tensor $[\alpha_{xyz}]$ is placed in an arbitrary field $\mathbf{F}$, an electric dipole $\mathbf{p}$ is induced:[61]

$$\mathbf{p} = 4\pi\epsilon_0[\alpha_{xyz}]\cdot\mathbf{F}. \tag{A2}$$

An electric dipole $\mathbf{p}$ in turn will generate an electric field $\mathbf{F_d}(\mathbf{r})$ at a position $\mathbf{r}$ relative to the dipole:[60]

$$\mathbf{F_d}(\mathbf{r}) = \frac{3(\mathbf{p}\cdot\mathbf{r})\mathbf{r} - \mathbf{p}r^2}{4\pi\epsilon_0 r^5}. \tag{A3}$$

Note that the polarizability volume tensor in global x,y,z coordinates $[\alpha_{xyz}]$ is linked to the molecular polarizability volume tensor in the local molecular coordinate system $[\alpha_{\mathrm{LMN}}]$ by[62]

$$[\alpha_{xyz}] = \mathbf{LMN}_{xyz}\cdot[\alpha_{\mathrm{LMN}}]\cdot\mathbf{LMN}_{xyz}^T, \tag{A4}$$

where $\mathbf{LMN}_{xyz}$ is the transformation matrix to transform a vector in local molecular coordinates (which is a right-handed orthonormal coordinate system with axes along the long, medium, and normal symmetry axes of the molecule, as defined in Ref. 37) into a vector in x,y,z coordinates. The three columns of $\mathbf{LMN}_{xyz}$ yield the unit vectors of the molecules long, medium, and normal axes expressed in x,y,z coordinates. In case of randomly oriented molecules, this transformation matrix will differ for each molecule. For pentacene,[37]

$$[\alpha_{\mathrm{LMN}}] = 4\pi\epsilon_0\begin{bmatrix} 78.22 & -6.879 & -4.531 \\ -6.879 & 31.31 & -2.322 \\ -4.531 & -2.322 & 25.51 \end{bmatrix} \times 10^{-24}\ \mathrm{C\ cm^2/V}. \tag{A5}$$

Now consider a distribution of $i=1\cdots n$ polarizable points (one point per submolecule) with vector position $\mathbf{r_i}$. A charge q is placed at position $\mathbf{r_0}$. At each point, the field equals the sum of the monopole field due to the charge, the fields due to the induced dipoles at all other points $j=1\cdots n, j\neq i$, and the fields due to possible permanent monopoles or dipoles:[63]

$$\mathbf{F_i} = \mathbf{F_m}(\mathbf{r_{i0}}) + \sum_{j\neq i}\mathbf{F_d}(\mathbf{F_{ij}}) + \sum \mathbf{F_{i,\text{permanent mono- or dipoles}}} \quad \text{for } \forall\, i, i\neq 0, \tag{A6}$$

where the vectors $\mathbf{r_{ij}}$ are defined as $\mathbf{r_i}-\mathbf{r_j}$. When written for all points and after inserting Eqs. (A1)–(A3) into Eq. (A6), a set of linear equations is described that can be solved for the fields $\mathbf{F_i}$ at each point. Gaussian elimination solves this set of equations directly. Alternatively, for translationally symmetric problems, it is possible to rewrite those equations and obtain the solution by the Fourier-transform method.[44,45] Knowing the self-consistent polarization fields (SCPF), the induced dipoles $\mathbf{p_i}$ at each point can be calculated from Eq. (A2). Finally, the polarization energy of the charge due to its interaction with induced dipoles is given by[64]

$$E_{q\text{-}id,r<R} = -\frac{1}{2}\sum_i \mathbf{p_i}\cdot\mathbf{F_m}(\mathbf{r_{i0}}), \tag{A7}$$

which must be increased by the interaction energy of the charge with possible permanent mono- or dipoles in the neighborhood (the interaction energy of the charge with permanent quadrupoles is discussed in the next section).[60]

In the present work, the linear set of equations in Eq. (A6) is solved by direct Gaussian elimination, using homebuilt MATLAB routines for up to about 2600 point dipoles on a desktop computer with 2 Gb of RAM memory. This corresponds to over 500 pentacene molecules with five submolecules each, e.g., all molecules in a three-dimensional crystal within a radius $R=35$ Å around the charged molecule. Calculations on (001) monolayers (two-dimensional crystals) are performed up to radii $R\leqslant 65$ Å.

The polarization energy contribution of all molecules in a *three-dimensional* crystal outside this radius R can be estimated either by extrapolating the results from smaller radii to $R=\infty$,[42,65] or by estimating the continuum polarization contribution as[45]

$$E_{q\text{-}id,r>R} = -\frac{q^2}{8\pi\epsilon_0 R}\left[1 - \frac{\left(\frac{1}{\epsilon_{xx}}+\frac{1}{\epsilon_{yy}}+\frac{1}{\epsilon_{zz}}\right)}{3}\right]. \tag{A8}$$

In case of pentacene, $\epsilon_{xx}=2.581$, $\epsilon_{yy}=3.471$, $\epsilon_{zz}=4.001$ (the xyz coordinate system was chosen such that the x-axis direction coincides with the [100] direction in the crystal lattice).[37] The continuum polarization contribution of all molecules within one *two-dimensional* monolayer outside radius R can be calculated using cylindrical coordinates in close analogy with Ref. 45 as

$$E_{q\text{-}id,r>R} = -\frac{q^2}{32\pi\epsilon_0 R}\left[\left(2-\frac{1}{\epsilon_{xx}}-\frac{1}{\epsilon_{yy}}\right)\times\int_{-c^*/2}^{c^*/2}\int_R^\infty \frac{r^3}{(r^2+z^2)^3}drdz + \left(2-\frac{2}{\epsilon_{zz}}\right)\times\int_{-c^*/2}^{c^*/2}\int_R^\infty \frac{z^2 r}{(r^2+z^2)^3}drdz\right], \tag{A9}$$

with c^* the monolayer thickness. Obviously, the contribution from all molecules outside a distance R from a charged molecule within just one monolayer is significantly smaller than the contribution from all molecules outside a distance R from a charged molecule in a three-dimensional bulk crystal. For the pentacene example, the monolayer contribution to the polarization energy from molecules outside a radius $R=35$ Å is only −0.014 eV, while the bulk crystal contribution from molecules outside this radius is −0.1422 eV. An alternative way to estimate the polarization energy contribution of all molecules in one crystalline *two-dimensional* monolayer outside a radius R is by extrapolating the expected scaling relation ($E_{q\text{-}id}\sim M^{-1}$, with M the number of molecules in a monolayer aggregate with radius R) to infinitely large aggregates. The scaling does not fit perfectly well, however, as can be seen in Fig. 9.

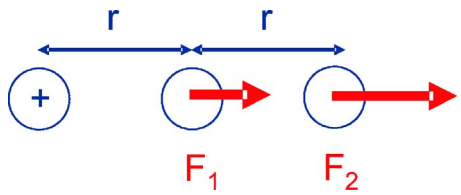

FIG. 8. (Color online) A positively charged nonpolarizable entity and two point polarizable entities at distances r from each other. For certain values of the isotropic polarizability α and distances r, the field can become larger with distance to the charge.

In the present work, molecules are modeled as a collection of s polarizable points equally distributed along the long symmetry axis of the molecule. Each polarizable point has a polarizability volume tensor $[\alpha_{\mathrm{LMN}}]/s$. The choice of s is restricted, as will be demonstrated by following simple analysis. Suppose a configuration in which a charge q and two polarizable points with isotropic polarizability α are placed in respective positions $\mathbf{r_0}=(0,0,0)$, $\mathbf{r_1}=(r,0,0)$, and $\mathbf{r}_2=(2r,0,0)$, as in Fig. 8. Solving Eq. (A6) for the electric fields $\mathbf{F}_1$ and $\mathbf{F}_2$ at the two polarizable points yields the following solution:

$$\mathbf{F_1} = \frac{1}{2}\frac{q}{4\pi\epsilon_0}\frac{r(2r^3+\alpha)}{r^6-4\alpha^2},$$

$$\mathbf{F_2} = \frac{1}{4}\frac{q}{4\pi\epsilon_0}\frac{r(r^3+8\alpha)}{r^6-4\alpha^2}. \tag{A10}$$

Intuitively, it is expected that the electric field decays with distance from the charge. This does not always seem to be the case, however. If α and r are chosen such that

$$\frac{\alpha}{3r^3} \geqslant 1 \tag{A11}$$

the electric field at the more distant polarizable point $\mathbf{r_2}$ can become *larger* than the field at $\mathbf{r_1}$. This phenomenon is related to ferroelectricity, where charge-induced dipoles are so strong that dipoles remain frozen in their states due to interactions with neighboring dipoles, even when the charge responsible for inducing the dipoles is taken away. Since pentacene is not known as a ferroelectric material, the number of polarizable points representing one molecule should be properly chosen in order to avoid this limit. For example, representing a pentacene crystal by one polarizable point per molecule with the full molecular polarizability concentrated to that point, i.e., $s=1$, will yield erroneous results with the presented self-consistent polarization field calculation, since $[\alpha_{\mathrm{LMN}}]$ will be too high given the distances between the centers of the molecules in a typical pentacene crystal. This phenomenon has been often confused with convergence problems.[11] When s is chosen higher, on the other hand, the polarizability volume tensor of each point, $[\alpha_{\mathrm{LMN}}]/s$, will become "diluted." Alternatively, when $[\alpha_{\mathrm{LMN}}]$ is lower, such as for benzene, naphtalene, and anthracene, a single point-polarizable entity per molecule is sufficient to calculate the polarization energy.[11] In order to prevent that this "ferroelectric" limit is crossed because the distance between polarizable points on the same molecule becomes smaller with increasing s, it might be necessary to exclude field contributions from points belonging to the same molecule in Eq. (A6). In the present work, s was chosen to be 5 for pentacene and 3 for anthracene (as indicated in between brackets following the calculated energies in Table I).

APPENDIX B: CHARGE-QUADRUPOLE INTERACTIONS

The interaction energy between a charge and a permanent quadrupole at a position $\mathbf{r_i}$ relative to the charge is given by[66,67]

$$E_{q\text{-}Q0} = -\frac{1}{3}\sum_{v}\sum_{w}\Theta_{vw}\frac{\partial F_{m,w}(\mathbf{r_i})}{\partial x_v}, \tag{B1}$$

with v and w addressing the x, y, and z coordinates of the global coordinate system. The total charge-quadrupole interaction energy of a charge in a matrix is simply the sum of the individual interactions between the charge and each permanent quadrupole in the matrix. The permanent quadrupole moment tensor in the global coordinate system, $[\Xi_{\mathrm{xyz}}]$, relates to the permanent quadrupole moment tensor in the local molecular coordinate system $[\Xi_{\mathrm{LMN}}]$ in the same way as the polarizability tensor in Eq. (A4). For one pentacene mol-

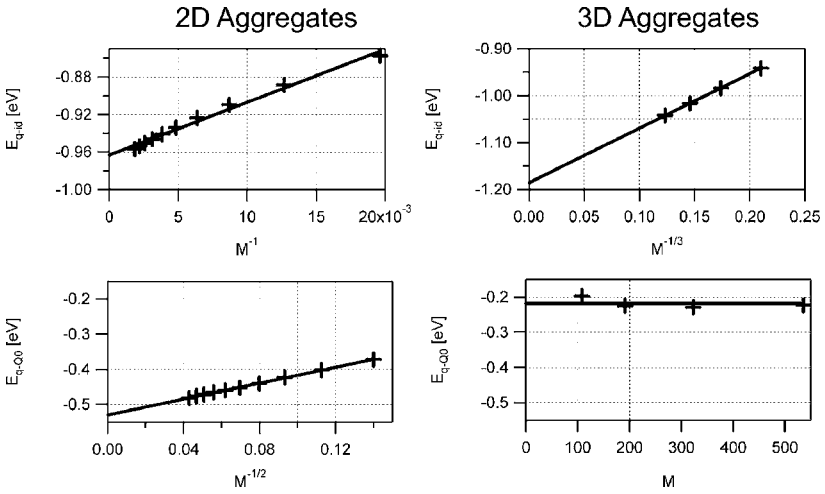

FIG. 9. Scaling relations for electronic polarization energy (top) and charge-quadrupole interaction energy (bottom) for two-dimensional (left) and three-dimensional (right) pentacene aggregates with the Siegrist *et al.* polymorph. The charge is located at the (1/2,1/2,0) position in each case.

ecule, the permanent quadrupole moment tensor is[37]

$$[\Theta_{LMN}] = \begin{bmatrix} 3.725 & 0 & 0 \\ 0 & 5.659 & 0 \\ 0 & 0 & -9.384 \end{bmatrix} \times 10^{-35}\ \mathrm{C\ cm^2}. \tag{B2}$$

As for the polarizability, the permanent quadrupole moment is distributed over s submolecules, each with a permanent quadrupole moment of $[\Xi_{LMN}]/s$. In Table I, s is indicated in between brackets following the calculated energies. When $s=3$ (for anthracene) or 5 (for pentacene), the permanent quadrupoles were distributed along the molecular long axis. When $s=14$ (for anthracene) or 22 (for pentacene), the permanent quadrupoles were distributed over all sp_2 hybridized carbon atoms. Since the latter results correspond better to more accurate calculations for atomic multipolar contributions to electronic polarization, $s=22$ has been used in the remainder of this work dealing with pentacene.

The charge-quadrupole contribution from one molecule scales with the distance r between the charge and the molecule like $\sim r^{-3}$. When summed over all molecules in a three-dimensional aggregate with radius R (containing $M \sim R^3$ molecules), it is found that overall, $E_{q\text{-}Q0}$ is more or less independent with three-dimensional aggregate size. For a monolayer aggregate with radius R on the other hand, $M \sim R^2$, resulting in $E_{q\text{-}Q0} \sim M^{-1/2}$. Those scaling relations are demonstrated in Fig. 9.

[1] E. A. Silinsh and V. Čápek, *Organic Molecular Crystals: Interaction, Localization, and Transport Phenomena* (AIP, New York, 1994).
[2] M. Pope and C. E. Swenberg, *Electronic Processes in Organic Crystals and Polymers*, 2nd ed. (Oxford University Press, New York, 1999), Chap. XIV, p. 963.
[3] V. M. Kenkre, J. D. Andersen, D. H. Dunlap, and C. B. Duke, Phys. Rev. Lett. **62**, 1165 (1989).
[4] G. Horowitz, D. Fichou, X. Peng, Z. Xu, and F. Garnier, Solid State Commun. **72**, 381 (1989).
[5] C. W. Tang, Appl. Phys. Lett. **48**, 183 (1986).
[6] C. W. Tang and S. A. VanSlyke, Appl. Phys. Lett. **51**, 913 (1987).
[7] Z.-T Zhu, J. T. Mason, R. Dieckmann, and G. G. Malliaras, Appl. Phys. Lett. **81**, 4643 (2002).
[8] J. E. Northrup and M. L. Chabinyc, Phys. Rev. B **68**, 041202(R) (2003).
[9] L.-L. Chua, J. Zaumseil, J.-F. Chang, E. C.-W. Ou, P. K.-H. Ho, H. Sirringhaus, and R. H. Friend, Nature (London) **434**, 194 (2005).
[10] J. Veres, S D. Ogier, S. W. Leeming, D. C. Cupertino, and S. M. Khaffaf, Adv. Funct. Mater. **13**, 199 (2003).
[11] E. A. Silinsh, *Organic Molecular Crystals—Their Electronic States* (Springer-Verlag, Berlin, 1980).
[12] K. Puntambekar, J. Dong, G. Haugstad, and C. Daniel Frisbie, Adv. Funct. Mater. **16**, 879 (2006).
[13] B. Nickel, R. Barabash, R. Ruiz, N. Koch, A. Kahn, L. C. Feldman, R. F. Haglund, and G. Scoles, Phys. Rev. B **70**, 125401 (2004).
[14] J. K. Kang, D. da Silva Filho, J.-L. Bredas, and X.-Y. Zhu, Appl. Phys. Lett. **86**, 152115 (2005).
[15] R. Ruiz, D. Choudhary, B. Nickel, T. Toccoli, K.-C. Chang, A. C. Mayer, P. Clancy, J. M. Blakely, R. L. Headrick, S. Iannotta, and G. G. Malliaras, Chem. Mater. **16**, 4497 (2004).
[16] J. Fraxedas, J. Caro, A. Figueras, P. Gorostiza, and F. Sanz, Surf. Sci. **415**, 241 (1998).
[17] M. C. J. M. Vissenberg and M. Matters, Phys. Rev. B **57**, 12964 (1998).
[18] P. G. Le Comber and W. E. Spear, Phys. Rev. Lett. **25**, 509 (1970).
[19] J. W. Orton and M. J. Powell, Rep. Prog. Phys. **43**, 1267 (1980).
[20] H. Nussbaumer, F. P. Baumgartner, G. Willeke, and E. Bucher, J. Appl. Phys. **83**, 292 (1998).
[21] S. Verlaak, V. Arkhipov, and P. Heremans, Appl. Phys. Lett. **82**, 745 (2003).
[22] C. Tanase, E. J. Meijer, P. W. M. Blom, and D. M. de Leeuw, Org. Electron. **4**, 33 (2003).
[23] E. J. Meijer, C. Tanase, P. W. M. Blom, E. van Veenendaal, B.-H. Huisman, D. M. de Leeuw, and T. M. Klapwijk, Appl. Phys. Lett. **80**, 3838 (2002).
[24] A. R. Völkel, R. A. Street, and D. Knipp, Phys. Rev. B **66**, 195336 (2002).
[25] R. A. Street, D. Knipp, and A. R. Völkel, Appl. Phys. Lett. **80**, 1658 (2002).
[26] A. Di Carlo, F. Piacenza, A. Bolognesi, B. Stadlober, and H. Maresch, Appl. Phys. Lett. **86**, 263501 (2005).
[27] Grain boundary models are generally less convenient to fit device characteristics given the fact that extensive two-dimensional device simulations are required to appropriately deal with the correct gate-voltage dependence of the trap occupation at grain boundaries.
[28] G. Horowitz and M. E. Hajlaoui, Adv. Mater. (Weinheim, Ger.) **12**, 14 (2000).
[29] T. W. Kelley, D. V. Muyres, P. F. Baude, T. P. Smith, and T. D. Jones, Mater. Res. Soc. Symp. Proc. **771**, L6.5.1 (2003).
[30] D. Knipp, R. A. Street, A. Völkel, and J. Ho, J. Appl. Phys. **93**, 1 (2003).
[31] G. Horowitz, M. E. Hajlaoui, and R. Hajlaoui, J. Appl. Phys. **87**, 4456 (2000).
[32] A. Dodabalapur, L. Torsi, and H. E. Katz, Science **268**, 270 (1995).
[33] F. Dinelli, M. Murgia, P. Levy, M. Cavallini, F. Biscarini, and D. de Leeuw, Phys. Rev. Lett. **92**, 116802 (2004).
[34] T. W. Kelley, L. D. Boardman, T. D. Dunbar, D. V. Muyres, M. J. Pellerite, and T. P. Smith, J. Phys. Chem. B **107**, 5877 (2003).
[35] S. Verlaak, C. Rolin, and P. Heremans, J. Phys. Chem. B **111**, 139 (2007).
[36] D. Tsiaousis and R. W. Munn, J. Phys. Chem. B **117**, 1833 (2002).
[37] I. Eisenstein and R. W. Munn, J. Chem. Phys. **77**, 47 (1983).
[38] J. Sworakowski, Mol. Cryst. Liq. Cryst. **19**, 259 (1973).
[39] S. Hayashi, I. Okada, N. Ide, and K. Kojima, J. Phys.: Condens. Matter **4**, L379 (1992).

[40] D. Tsiaousis and R. W. Munn, J. Chem. Phys. **117**, 10860 (2002).
[41] R. W. Munn, Mol. Cryst. Liq. Cryst. Sci. Technol., Sect. A **228**, 23 (1993).
[42] E. V. Tsiper and Z. G. Soos, Phys. Rev. B **68**, 085301 (2003).
[43] N. Sato, H. Inokuchi, and E. A. Silinsh, Chem. Phys. **115**, 269 (1987).
[44] P. J. Bounds and R. W. Munn, Chem. Phys. **59**, 47 (1981).
[45] D. B. Knowles and R. W. Munn, J. Mater. Sci.: Mater. Electron. **5**, 89 (1994).
[46] Z. G. Soos, E. V. Tsiper, and R. A. Pascal Jr., Chem. Phys. Lett. **342**, 652 (2001).
[47] S. Verlaak, S. Steudel, P. Heremans, D. Janssen, and M. S. Deleuze, Phys. Rev. B **68**, 195409 (2003).
[48] L. F. Drummy, P. K. Miska, D. Alberts, N. Lee, and D. C. Martin, J. Phys. Chem. B **110**, 6066 (2006).
[49] H. S. Lee, D. H. Kim, J. H. Cho, Y. D. Park, J. S. Kim, and K. Cho, Adv. Funct. Mater. **16**, 1859 (2006).
[50] D. R. Desiraju and T. Steiner, *The Weak Hydrogen Bond*, 1st ed. (Oxord University Press, Oxford, 1999).
[51] D. P. Craig and B. R. Markey, Mol. Cryst. Liq. Cryst. **58**, 77 (1980).
[52] D. P. Craig and B. R. Markey, Chem. Phys. Lett. **62**, 223 (1979).
[53] J. R. Fryer and D. J. Smith, Proc. R. Soc. London, Ser. A **381**, 225 (1982).
[54] F. Biscarini, E-MRS spring meeting, Strasbourg, France, 2003 (unpublished).
[55] J. E. Northrup, M. L. Tiago, and S. G. Louie, Phys. Rev. B **66**, 121404(R) (2002).
[56] Z.-T. Zhu, J. T. Mason, R. Dieckmann, and G. Malliaras, Appl. Phys. Lett. **81**, 4643 (2002).
[57] B. Crone, A. Dodabalapur, A. Gelperin, L. Torsi, H. E. Katz, A. J. Lovinger, and Z. Bao, Appl. Phys. Lett. **78**, 2229 (2001).
[58] B. K. Crone, A. Dodabalapur, R. Sarpeshkar, A. Gelperin, H. E. Katz, and Z. Bao, J. Appl. Phys. **91**, 10140 (2002).
[59] S. Verlaak, Ph.D. thesis, KULeuven, Leuven, 2004, Chap. 3.
[60] J. D. Jackson, *Classical Electrodynamics*, 3rd ed. (Wiley, New York, 1999).
[61] P. W. Atkins, *Physical Chemistry*, 6th ed. (Oxford University Press, Oxford, 1998).
[62] D. E. Sands, *Vectors and Tensors in Crystallography* (Addison-Wesley, Reading, MA, 1982).
[63] Permanent higher-order multipoles can be incorporated in the same way. However, their fields drop even faster with distance than permanent dipoles (Ref. 61). Therefore the higher the order of the permanent multipole, the more localized their impact on the SCPF calculation.
[64] S. D. Druger and R. S. Knox, J. Chem. Phys. **50**, 3143 (1969).
[65] The polarization energy contribution $\sim \mathbf{p_i F_m} \sim r^{-4}$ should be summed over the total number of molecules $M \sim R^3$ in a three-dimensional aggregate of radius R: $\sim \int \frac{1}{r^4} \pi r^2 dr$, resulting in an overall scaling behavior of $E_{q-id} \sim r^{-1} \sim M^{-1/3}$.
[66] P. J. Bounds and R. W. Munn, Chem. Phys. **59**, 41 (1981).
[67] Please note that this formula may differ by a factor of 2 depending on the definition of the quadrupole moment tensor, e.g., when compared to Ref. 60. The present expression is consistent with the quadrupole moment tensor that is used here.
[68] R. B. Campbell, J. M. Robertson, and J. Trotter, Acta Crystallogr. **15**, 289 (1962).
[69] T. Siegrist, C. Kloc, J. H. Schön, B. Batlogg, R. C. Haddon, S. Berg, and G. A. Thomas, Angew. Chem., Int. Ed. **40**, 1732 (2001).
[70] R. Mason, Acta Crystallogr. **17**, 547 (1964).
[71] Z. G. Soos and E. V. Tsiper, Macromol. Symp. **212**, 1 (2004).
[72] J. M. Sin, E. V. Tsiper, and Z. G. Soos, Europhys. Lett. **60**, 743 (2002).
[73] C. P. Brock and J. D. Dunitz, Acta Crystallogr., Sect. B: Struct. Sci. **46**, 795 (1990).